A Synchronous Reference Frame PI Current Controller With Dead Beat Response

Claudio A. Busada, Sebastian Gomez Jorge, and Jorge A. Solsona, *Senior Member, IEEE*

***Abstract*—In this paper, a new structure of a proportional integral (PI) current controller implemented in a synchronous d, q reference frame (SRF-PI), for grid-tied voltage inverters, is presented. The controller has deadbeat response for current reference tracking, reaching it in two samples. It also keeps the main feature of the SRF-PI controller: its ability to track without error, in the absence of other disturbances, a positive sequence current reference of fundamental frequency. Furthermore, the controller ensures the full decoupling between the currents of axes d and q. The controller is compared, through simulation and experimental results, with one SRF-PI controller recently published in the literature. It is verified that the proposed controller introduces noticeable improvements in both the transient response and in the steady-state response to perturbations in the control loop.**

***Index Terms*—Current control, digital current control system, proportional integral (PI), real and reactive power control, synchronous *d–q* frame.**

I. Introduction

VOLTAGE source inverters (VSI) are widely used in the injection of renewable resources into distribution networks. In order to comply with the increasingly restrictive interconnection standards, VSI current control becomes an increasingly relevant issue [1]. The control must not only provide currents with low total harmonic distortion (THD) [2], but also must present an excellent dynamic response to meet the required response times [3], [4].

A high-performance current controller, which at the same time is characterized by the simplicity of its implementation, is the predictive dead beat [5], [6]. In the digital signal processor (DSP) implementation of this controller, it is possible to achieve the control objective in a time of two samples. It also allows us to follow arbitrarily fast references, with a delay of only two samples. In its basic form, the performance of the dead beat controller is affected by the uncertainties in the plant model [7], [8] and offers low rejection of nonmodeled disturbances.

Manuscript received December 10, 2018; revised April 25, 2019; accepted June 23, 2019. Date of publication June 27, 2019; date of current version December 13, 2019. This work was supported by the Universidad Nacional del Sur, CONICET and ANPCyT, Argentina. Recommended for publication by Associate Editor B. G. Fernandes. *(Corresponding author: Sebastian Gomez Jorge.)*

The authors are with the Instituto de Investigaciones en Ingeniería Eléctrica and the Departamento de Ingeniería Eléctrica y de Computadoras, Universidad Nacional del Sur-CONICET, Bahía Blanca 8000, Argentina (e-mail: cbusada@uns.edu.ar; sebastian.gomezjorge@uns.edu.ar; jsolsona@uns.edu.ar).

Color versions of one or more of the figures in this paper are available online at http://ieeexplore.ieee.org.

Digital Object Identifier 10.1109/TPEL.2019.2925705

A very popular current controller is the proportional plus resonant (PR), which is implemented in a stationary α, β reference frame. Lately, several efforts have been made to improve the dynamic response of the PR controllers [9]–[11]. In [12], it is verified that it is theoretically possible to obtain a dead beat response with them. However, these controllers have the disadvantage of presenting coupling between the injected active and reactive power (p and q): a change of p affects q, and vice versa. These controllers are naturally decoupled in the α, β frame, but coupled in a synchronous d, q reference frame oriented with the fundamental component of the grid voltage.

Another widely used current controller is the proportional-integral (PI) controller, implemented in a synchronous d, q reference frame (SRF-PI) [13]. The controller offers infinite rejection to disturbances of fundamental frequency and positive sequence, and can follow without error a current reference of these characteristics (in the absence of disturbances at other frequencies). Because it is implemented in an SRF, it has the advantage of being able to decouple the changes of p from the changes of q [14], [15], providing a precise control of these magnitudes. Although the SRF-PI is one of the most widespread controllers, it is still of interest to optimize its response, in terms of settling time and overshoot [16]. In [17], guidelines for designing an SRF-PI in discrete time are presented. In order to improve the controller response, it is very important to properly include the rotation speed of the SRF in the controller design.

In a recent publication [18], Hoffmann *et al.* present a PI controller formulated in discrete time, capable of fully decoupling axes d and q [19]. However, the proposal does not provide full control of the location of the closed-loop poles of the system. This limits, as will be seen here, the speed with which the controller can cancel the effect of a disturbance in the control loop. For various reasons, it is desirable that the controller is quick to cancel such disturbances. For example, modern grid codes dictate the injection of specific amounts of reactive current within a maximum period of time after a fault occurrence [3], [4].

In this paper, a new controller structure and design methodology for the SRF-PI is presented. As in [18], the proposed SRF-PI is formulated in discrete time and it ensures full decoupling between axes d and q. However, the proposed SRF-PI controller presents the novelty of being able to attain a dead beat response for current reference tracking. Thus, it combines the advantages of the standard SRF-PI with the advantages of the dead beat, both in a single controller. From the SRF-PI, the controller inherits its ability to track without error a positive sequence current reference of fundamental frequency (in the absence of other

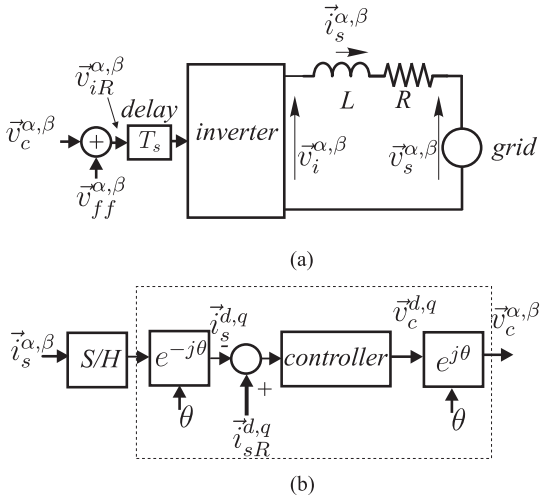

Fig. 1. (a) System. (b) Controller scheme.

disturbances), and its ability to decouple axes d and q. From the dead beat controller, the proposal inherits its speed: the ability to reach and track an arbitrary current reference, with a delay of only two samples. In addition, the controller designer has full control over the location of the closed-loop poles of the system. This allows us to quickly cancel perturbations in the control loop, and additionally improve the steady-state rejection capabilities. To put the proposal in context with the state of the art, the proposed controller is compared with that in [18], both through simulations and experiments.

II. System Model

Fig. 1(a) shows a three-phase inverter, connected to the grid through an *R–L* series circuit. In this paper, the variables are expressed using complex notation. Variables $\vec{v}_i^{\alpha,\beta} = v_i^\alpha + jv_i^\beta$ and $\vec{v}_s^{\alpha,\beta} = v_s^\alpha + jv_s^\beta$ represent the voltage imposed by the inverter and the grid, respectively, in the stationary α,β reference frame. The behavior of the current flowing through the *R–L* circuit is described by $Ld\vec{i}_s^{\alpha,\beta}/dt + \vec{i}_s^{\alpha,\beta}R = \vec{v}_i^{\alpha,\beta} - \vec{v}_s^{\alpha,\beta}$ where $\vec{i}_s = i_s^\alpha + ji_s^\beta$ is the current in the inductor. As shown in Fig. 1(a), reference $\vec{v}_{iR}^{\alpha,\beta}$ imposed to the pulsewidth modulator (PWM) is the sum of $\vec{v}_{ff}^{\alpha,\beta}$ with $\vec{v}_c^{\alpha,\beta}$ where $\vec{v}_{ff}^{\alpha,\beta}$ is a feedforward voltage used to partially cancel the effect of $\vec{v}_s^{\alpha,\beta}$ on $\vec{i}_s^{\alpha,\beta}$, and $\vec{v}_c^{\alpha,\beta}$ represents the control action imposed by the current controller. The presence of cancellation voltage $\vec{v}_{ff}^{\alpha,\beta}$ is not mandatory in SRF-PI controllers.

The proposed controller will be implemented in discrete time in a DSP, using a sampling period T_s. Fig. 1(a) assumes that there is a one sample delay (T_s) between the calculation of control action $\vec{v}_{iR}^{\alpha,\beta}$ and the actual application of this voltage at the inverter output. In order to design the controller, the plant model must be discretized. Note that the zero-order hold (ZOH) action is carried out by the PWM of the VSI (which lies naturally in the stationary frame). This suggest that the ZOH discretization of the plant must be carried out in the stationary frame. This is so, even when the current controller is to be implemented in a synchronous frame. Once the plant is discretized in the stationary frame, the design of the controller requires transforming this model to the synchronous frame. Modeling the inverter as a unity gain, the ZOH discretization of the system of Fig. 1(a) results [17]

$$\vec{i}_s^{\alpha,\beta}(k+1) = a\vec{i}_s^{\alpha,\beta}(k) + b\left[\vec{v}_o^{\alpha,\beta}(k) + \vec{v}_p^{\alpha,\beta}(k)\right] \quad (1)$$

$$\vec{v}_o^{\alpha,\beta}(k+1) = \vec{v}_c^{\alpha,\beta}(k) \quad (2)$$

where k is the sample number, $a = e^{-RT_s/L} \in \Re$, $b = (1-a)/R \in \Re$, $\vec{v}_o^{\alpha,\beta}(k)$ defined in (2) is a dummy variable (represents $\vec{v}_c^{\alpha,\beta}$ delayed one sample), and

$$\vec{v}_p^{\alpha,\beta}(k) = \vec{v}_{ff}^{\alpha,\beta}(k-1) - \vec{v}_s^{\alpha,\beta}(k) \quad (3)$$

represents a disturbance voltage, with $\vec{v}_s^{\alpha,\beta}(k)$ the average value of $\vec{v}_s^{\alpha,\beta}(t)$ over the interval $kT_s \le t < (k+1)kT_s$ [12]. Because constants a and b of (1) are real numbers, the behavior of axes α and β of (1) is independent of each other. It is thus verified that in the α,β frame, both axes are decoupled from each other.

Fig. 1(b) outlines a controller implemented in a synchronous d,q frame, shifted an angle $\theta(k)$ from the α,β frame. Signal $\vec{i}_s^{d,q}$ is the d,q representation of signal $\vec{i}_s^{\alpha,\beta}(k)$, and $\vec{i}_{sR}^{d,q}$ is the reference for this current. Signal $\vec{v}_c^{d,q}$ is the controller output. In order to design the controller, it is necessary to transform (1)–(2) into the d,q frame. It is known that if $\vec{f}$ is a generic variable, the d,q and α,β representations of $\vec{f}$ are related through: $\vec{f}^{d,q}(k) = \vec{f}^{\alpha,\beta}(k)e^{-j\theta(k)}$, $\vec{f}^{d,q}(k+1) = \vec{f}^{\alpha,\beta}(k+1)e^{-j[\theta(k)+\omega_g T_s]}$, where ω_g is the average d,q frame rotation frequency, between interval k and $k+1$. Applying this to (1)–(2), its d,q frame representation results

$$\vec{i}_s^{d,q}(k+1) = a_g\vec{i}_s^{d,q}(k) + b_{g1}\left[\vec{v}_o^{d,q}(k) + \vec{v}_p^{d,q}(k)\right] \quad (4)$$

$$\vec{v}_o^{d,q}(k+1) = b_{g2}\vec{v}_c^{d,q}(k) \quad (5)$$

where

$$a_g = ae^{-j\omega_g T_s} \in C \quad (6)$$

$$b_{g1} = be^{-j\omega_g T_s} \in C \quad (7)$$

$$b_{g2} = e^{-j\omega_g T_s} \in C. \quad (8)$$

The fact that constants a_g, b_{g1}, and b_{g2} are complex numbers, indicates that the axes of system (4)–(5) are coupled [14]. The z transform of (4)–(5) results

$$\vec{i}_s^{d,q}(z) = \frac{b_{g1}b_{g2}}{z(z-a_g)}\vec{v}_c^{d,q}(z) + \frac{b_{g1}}{z-a_g}\vec{v}_p^{d,q}(z). \quad (9)$$

III. Recently Proposed Decoupled Controller

Based on the continuous time model of the *R–L* plant, the decoupling of axes d and q is usually performed by adding the feedforward term $j\omega_g L\vec{i}_s^{d,q}$ to the control action [15]. However, (4)–(5) show that this method is not effective when the processing delay and the ZOH discretization of the plant are taken into account. Hoffmann *et al.* [18] propose a decoupled controller

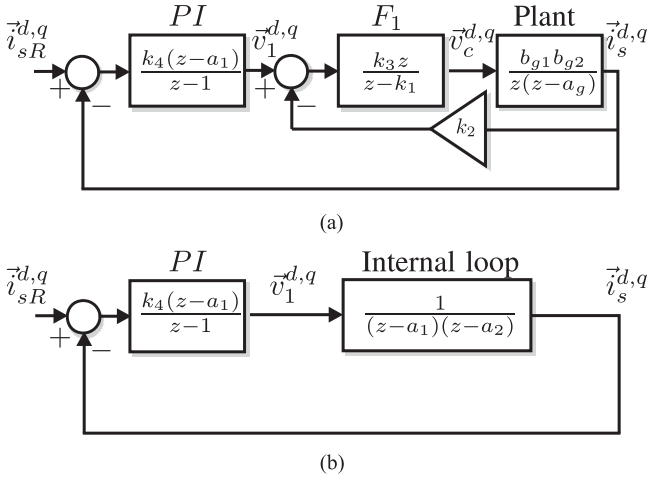

Fig. 2. (a) Proposed controller block diagram. (b) Equivalent controller block diagram.

that takes these into account. In that paper, the following SRF-PI controller is proposed:

$$\frac{\vec{v}_c^{d,q}(z)}{\vec{i}_{sR}^{d,q}(z)-\vec{i}_s^{d,q}(z)} = \gamma b_{g1}^{-1} b_{g2}^{-1} \frac{z-a_g}{z-1} \tag{10}$$

where $\gamma \in \Re$ is a constant. Applying this controller to (9) the following closed-loop system is obtained:

$$\vec{i}_s^{d,q}(z) = \underbrace{\frac{\gamma}{z^2-z+\gamma}}_{G_R(z)} \vec{i}_{sR}^{d,q}(z) + \underbrace{\frac{b_{g1}(z-1)z}{(z^2-z+\gamma)(z-a_g)}}_{G_P(z)} \vec{v}_p^{d,q}(z). \tag{11}$$

Transfer function $G_R(z)$ defined in (11) has real coefficients, which indicates a perfect decoupling between axes d and q when there is no perturbation ($\vec{v}_p^{d,q}=0$). With $\gamma = 0.3$, the closed-loop step response has an overshoot of 1% and a settling time, to 5% of the final value, of only 6 samples [18].

Transfer function $G_P(s)$ defined in (11) has the same poles as $G_R(s)$, plus a pole located at $z = a_g = e^{-(\frac{R}{L}+j\omega_g)T_s}$. In a predominantly inductive *R–L* circuit, this pole is poorly damped. Therefore, in general, the closed-loop system will have a slow response to a variation in perturbation $\vec{v}_p^{d,q}$.

IV. Proposed Controller

In what follows, the proposed dead beat controller is presented. First, the case $\vec{v}_p^{d,q}=0$ is considered, because this disturbance does not intervene in the design of the controller. Fig. 2(a) shows a block diagram of the proposed controller. Block "Plant" represents the system to control, defined by (9) with $\vec{v}_p^{d,q}=0$. The controller has two loops, one external and the other internal. The external loop is composed of a PI controller that has a pole at $z=1$ and one zero. The internal loop involves transfer function $F1$, that has one zero at $z=0$ and one pole. The internal loop will be responsible for producing the decoupling between axes d and q of the system and relocating the poles to suitable locations. The external loop will regulate the current to the reference value, with zero dc error. To verify that the internal loop is able to achieve the decoupling between the axes and of repositioning the poles, the closed-loop transfer function between intermediate signal $\vec{v}_1^{d,q}$ defined in Fig. 2(a) and current $\vec{i}_s^{d,q}$ is computed

$$\frac{\vec{i}_s^{d,q}(z)}{\vec{v}_1^{d,q}(z)} = \frac{\overbrace{k_3 b_{g1} b_{g2}}^{\kappa_0}}{z^2 - \underbrace{(k_1+a_g)}_{\lambda_1} z + \underbrace{k_2 k_3 b_{g1} b_{g2} + k_1 a_g}_{\lambda_0}}. \tag{12}$$

Note that properly choosing the values of gains k_1–k_3, coefficients λ_0, λ_1, and κ_0 of (12) can be given arbitrary values. If these coefficients are real, it is guaranteed that both axes are decoupled [14]. For example, let $a_1 \in \Re$, $|a_1|<1$ and $a_2 \in \Re$ be two constants selected by the designer, and choose k_1–k_3 as follows:

$$k_1 = a_1 + a_2 - a_g \tag{13}$$

$$k_2 = a_1 a_2 - k_1 a_g \tag{14}$$

$$k_3 = b_{g1}^{-1} b_{g2}^{-1}. \tag{15}$$

With this choice, the closed-loop system (12) results

$$\frac{\vec{i}_s^{d,q}(z)}{\vec{v}_1^{d,q}(z)} = \frac{1}{z^2-(a_1+a_2)z+a_1 a_2} = \frac{1}{(z-a_1)(z-a_2)}. \tag{16}$$

The resulting system is completely decoupled, since all the coefficients involved in (16) are real numbers. The poles are relocated to $z=a_1$ and $z=a_2$ along the real axis in the z plane. This verifies that the internal loop is capable of decoupling axes d and q and relocating the poles.

The external loop will now be analyzed, after choosing k_1–k_3 according to (13)–(15). Fig. 2(b) shows this loop, replacing the internal loop by its equivalent transfer function (16). Note that the zero of the PI is set at $z=a_1$, so that it is canceled with one of the poles of (16). For the cancelation to be stable, $|a_1|<1$ must be satisfied. Then, the closed-loop transfer function of the system of Fig. 2(b) results

$$\frac{\vec{i}_s^{d,q}(z)}{\vec{i}_{sR}^{d,q}(z)} = \frac{k_4}{z^2 - \underbrace{(a_2+1)}_{\zeta_1} z + \underbrace{k_4+a_2}_{\zeta_2}}. \tag{17}$$

Note from (17) that choosing constants a_2 and k_4 properly, it is possible to arbitrarily assign coefficients ζ_1 and ζ_2 of (17), and therefore, its poles. To obtain a dead beat controller, the two closed-loop poles of (17) must be located at $z=0$ [20]. To achieve this, $a_2=-1$ and

$$k_4 = 1 \tag{18}$$

must be chosen. This results in $\zeta_1=\zeta_2=0$. Doing this, the constants defined in (13)–(15) of the internal loop result

$$k_1 = a_1 - 1 - a e^{-j\omega_g T_s} \tag{19}$$

$$k_2 = -k_1 a e^{-j\omega_g T_s} - a_1 \tag{20}$$

$$k_3 = \frac{e^{j2\omega_g T_s}}{b} \tag{21}$$

where (13)–(15) were used along with (6)–(8). The design of the dead beat controller requires only the designer's choice of constant $a_1 \in \Re,\ |a_1| < 1$, and knowledge of parameters a and b of the discrete representation of the plant in the stationary α, β frame [see (1)]. Once constant a_1 is chosen, constants k_1–k_4 of the controller must be computed according to (18)–(21).

Constant a_1 defines the position of the pole that is canceled with the zero of the PI. Such cancellation means that its choice does not affect the transfer function $\vec{i}_s^{d,q}/\vec{i}_{sR}^{d,q}$.

Considering now the perturbation input $\vec{v}_p^{d,q}$ presented in (9), it is easy to verify that the closed-loop behavior of the system is described by

$$\vec{i}_s^{d,q}(z) = \underbrace{\frac{1}{z^2}}_{G'_R(z)} \vec{i}_{sR}^{d,q}(z) + \underbrace{\frac{b_{g1}(z-1)(z-k_1)}{z^2(z-a_1)}}_{G'_P(z)} \vec{v}_p^{d,q}(z). \quad (22)$$

Transfer function $G'_P(z)$ defined in (22) has the same poles as $G'_R(z)$, plus one pole located at $z = a_1$. Unlike what happens in (11) where the additional pole location is defined by the time constant of the *R–L* plant, in (22), the location of the pole is defined by the designer by appropriately choosing a_1. If $|a_1|$ is small, the closed-loop response of the system to a variation in perturbation $\vec{v}_p^{d,q}$ is fast. However, as shown in the next section, making this constant too small makes the control action more susceptible to saturation in the presence of a disturbance.

Comment 1: It is worth mentioning that the constants defined in (19)–(21) are dependent on the frequency of the grid ω_g, and can be adjusted online. However, in grid injection applications, if these constants are calculated at nominal frequency and not adjusted online, the closed-loop response does not degrade significantly. This is because in these applications, the frequency is kept in a small neighborhood around its nominal value. The online update of the controller gains with the frequency is necessary when the SRF-PI is used in machine drive applications where the frequency varies in a wider range.

Comment 2: Although this paper focuses on obtaining a dead beat response, it is possible to arbitrarily assign the values of coefficients ζ_1 and ζ_2 of (17) following the presented design procedure. For example, if a slower response than that of the dead beat is desired, to the effect of reducing the magnitude of the control action during abrupt changes in the reference, you can choose in (17) $a_2 = z_p - 1$, with $0 \leq z_p < 1 \in \Re$, and $k_4 = -a_2$. With this choice, (17) results

$$G'_R(z) = \frac{\vec{i}_s^{d,q}(z)}{\vec{i}_{sR}^{d,q}(z)} = \frac{1 - z_p}{z(z - z_p)} \quad (23)$$

which places one pole at the origin and the other at $z = z_p$. The system now behaves as a first-order system, in series with a unit delay. The proposed design procedure also allows us to obtain $G'_R(z) = G_R(z)$, with $G_R(z)$ defined in (11). To do so, $a_2 = 0$ and $k_4 = \gamma$ must be chosen.

V. Simulation Results

The proposed dead beat controller will now be simulated, and compared with the controller proposed in [18, see (10)]. Gains $k_1 - k_4$ of the proposed controller were obtained from (18)–(21), after choosing $a_1 = 0.75$. Controller (10) was designed with $\gamma = 0.3$ (the same value used in [18]).

The schematic of the simulated system is shown in Fig. 1(a). The parameters of the system are the following: $L = L^{\text{nom}} = 4.5\,\text{mH}$, $R = R^{\text{nom}} = 676.66\ \text{m}\Omega$, $T_s = 100\,\mu\text{s}$, the grid voltage is sinusoidal with 110 Vrms and angular fundamental frequency $\omega_g = 2\pi 50$ rad/s. The VSI is simulated as a unity gain controlled voltage source (no switching is included). The synchronism with the fundamental component of the grid voltage is achieved using an SRF-PLL [21]. To test the behavior of the closed-loop system to a perturbation input, the method proposed in [12] will be used. For this, voltage $\vec{v}_{ff}^{\alpha,\beta}$ [see Fig. 1(a)] is made proportional to the fundamental component of the grid voltage (called hereafter $\vec{v}_{s0}^{\alpha,\beta}$), provided by SRF-PLL. That is, $\vec{v}_{ff}^{\alpha,\beta} = K\vec{v}_{s0}^{\alpha,\beta}$, where K is a constant. With this, the perturbation voltage (3) applied to the control loop results

$$\vec{v}_p^{\alpha,\beta}(k) = K\vec{v}_{s0}^{\alpha,\beta}(k-1) - \vec{v}_s^{\alpha,\beta}(k). \quad (24)$$

An easy way to subject the system to a controlled variation of perturbation $\vec{v}_p^{\alpha,\beta}$ is to introduce a variation in K.

Simulation 1: The response of the proposed controller to a variation in current references $\vec{i}_{sR}^{d,q} = i_{sR}^d + ji_{sR}^q$ is first simulated. For the whole simulation, $K = 1$ was used in (24). Fig. 3 (a) and (b) shows the results. Fig. 3(a) shows the phase currents, and Fig. 3(b) shows the current references i_{sR}^d and i_{sR}^q (dashed line), along with currents i_s^d and i_s^q (solid lines). The simulation starts with the current references $i_{sR}^d = 10$ A and $i_{sR}^q = 0$ A, injecting 2.33 kW of active power and no reactive power to the grid. At $t = t_1$, the current reference of the d-axis i_{sR}^d is reduced from 10 to 5 A. Current i_s^d copies this reference in two samples, reaching 5 A. As shown in Fig. 3(b), the current of the q-axis is not affected by this reference change of the d-axis. 10 ms after this event, at $t = t_2$, the current reference of the q axis, i_{sR}^q, is increased from 0 to 2.5 A. Fig. 3(b) shows that current i_s^q copies this reference in two samples. It is observed that in this case, the current of the d-axis is not affected by the change of the current of the q-axis. This verifies the ability to reach the current reference in only two samples and the decoupling between axes.

This simulation was repeated for controller (10). Fig. 3(c) and (d) shows the results. As expected, it is verified that the current references are reached after six samples, with an overshoot of 1%. The decoupling between the axes is also verified. As shown by the results, controller (10) has a very good transient response to current reference changes.

Simulation 2: For this simulation, the grid voltage was contaminated with the following harmonics: 5th (3%), 7th (2%), 11th (0.3%), and 13th (0.3%) (THD = 3.63%). With this voltage, the system is simulated until steady state is reached. Fig. 4 (a) (top) shows the applied grid voltage, 4(a) (middle) shows the current injected by the proposed controller (THD = 1.91%), and 4(a) (bottom) shows the current injected by controller (10) (THD = 4.65%). As can be seen, the proposed controller has better steady-state disturbance rejection than (10), for the value of a_1 chosen by design. To justify this difference, the magnitudes (in [dB]) of the frequency responses of $G_P(z)$ [defined in (11)] and $G'_P(z)$ [defined in (22)] were plotted together in Fig. 4(b),

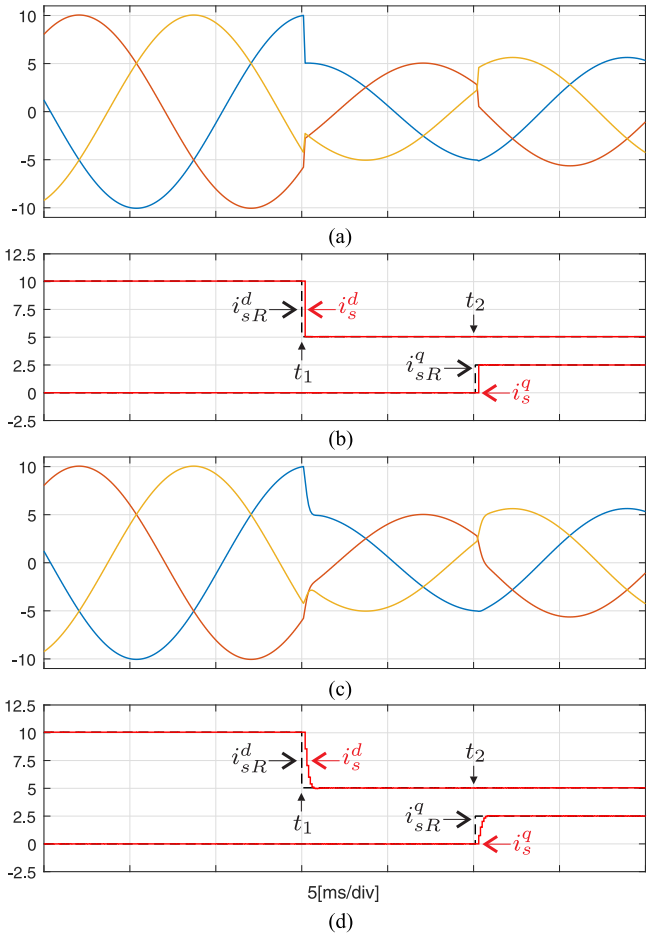

Fig. 3. Simulation results to reference changes. (a) Phase currents for proposed controller (in [A]). (b) Current references i^d_{sR} and i^q_{sR} (dashed) and currents i^d_s and i^q_s (solid) for proposed controller (in [A]). (c) and (d) same results as (a) and (b) for controller (10).

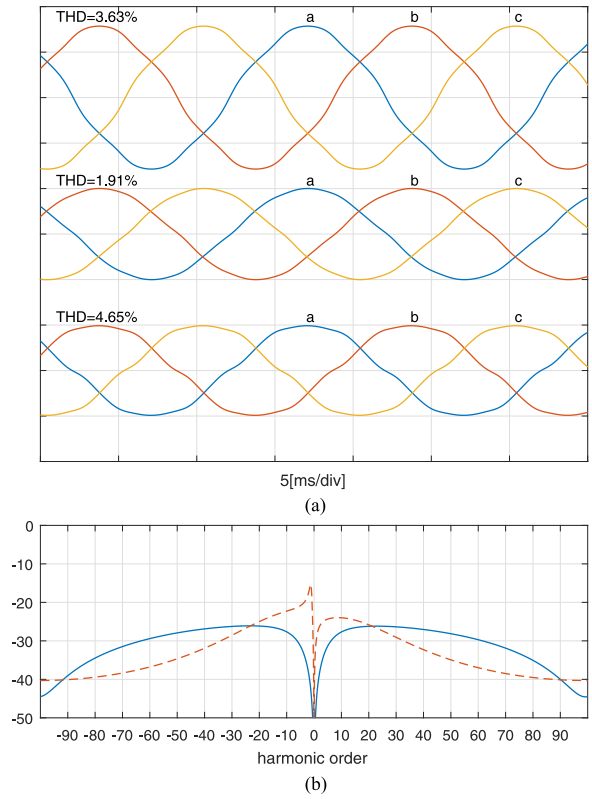

Fig. 4. Simulation results in steady state. (a) Phase voltages (top, scale 100 V/div), current injected by the proposed controller (middle, scale 10 A/div) and current injected by controller (10) (bottom, scale 10 A/div). (b) Magnitude of Bode plots (in [dB]) of G'_p (solid) and G_p (dashed).

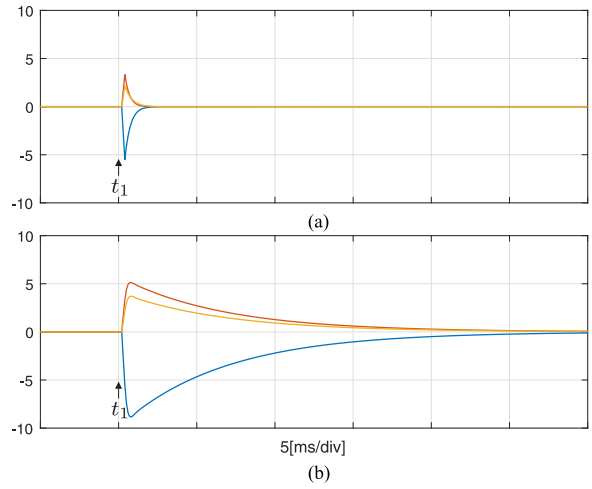

Fig. 5. Simulation results to a step change in K. (a) Phase currents for proposed controller (in [A]). (b) Phase currents for controller (10) (in [A]).

as a function of the harmonic order. It can be seen that up to the 20th harmonic where most of the contamination is located in realistic grids, the proposed controller has better steady-state disturbance rejection capabilities. Above that harmonic order, the opposite happens.

Simulation 3: The dynamic responses of both controllers to a variation in perturbation $\vec{v}_p^{\alpha,\beta}$ was simulated. For each controller, the reference was set to $i^d_{sR} = i^q_{sR} = 0$ A during the whole simulation. Initially, for $t < t_1$, $K = 1$ was used in the feedforward term. Then, at $t \geq t_1$, K is set to 0. Fig. 5 (a) shows the behavior of the currents using the proposed controller. It can be seen that the disturbance at $t = t_1$ results in a transient current that deviates from the reference current. As can be seen, the currents take 1.24 ms to reach 5% of the peak value of the transient. Fig. 5(b) shows the same results for controller (10). Using this controller, the currents take 20.52 ms to reach 5% of the peak value of the transient. It is verified that the proposed controller has faster rejection to disturbance $\vec{v}_p^{\alpha,\beta}$ than (10). Controller (10) is noticeably slower in this regard, mainly due to the poor damping of the pole in transfer function $G_P(z)$ of (11), located at $z = a_g$. Transfer function $G'_P(z)$ of (22), on the other hand, has two poles at the origin and one at $z = a_1$, in a well damped position.

A. Sensitivity Analysis

In order to analyze with more depth, the effect of the value of a_1 in the behavior of the closed-loop system, the sensitivity function S and the complementary sensitivity function $T = 1 - S$

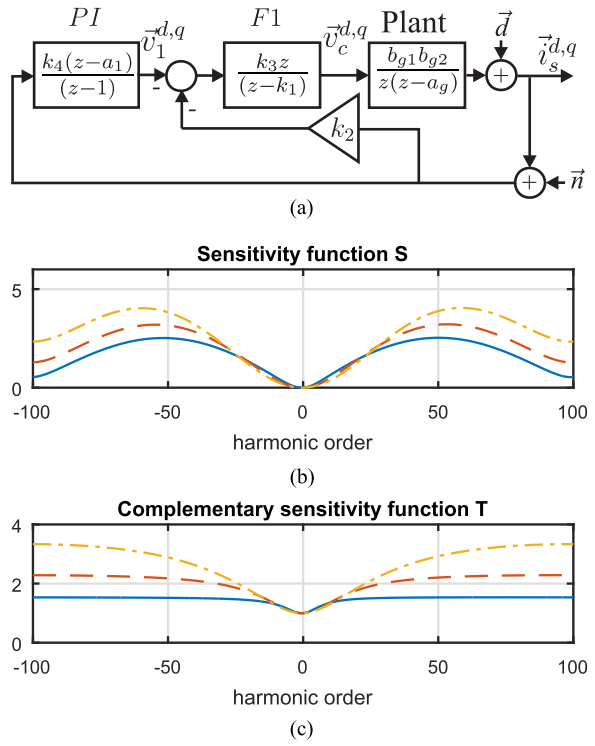

Fig. 6. (a) System block diagram used to obtain S and T. (b) Sensitivity function. (c) Complementary sensitivity function. $a_1 = 0.75$ (solid), $a_1 = 0.5$ (dash), and $a_1 = 0.25$ (dash dot).

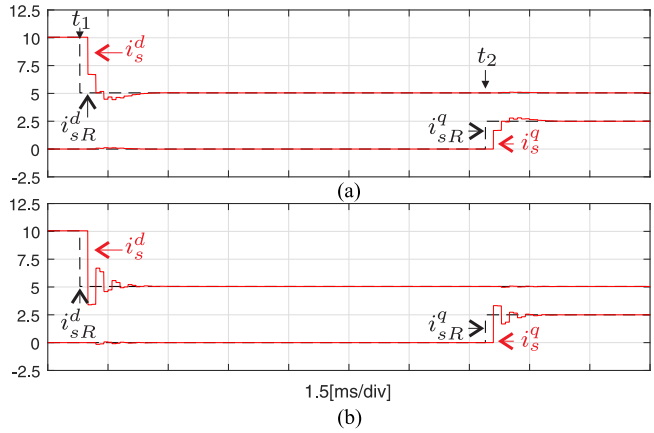

Fig. 7. Parameter mismatch. (a) Current references i_{sR}^d and i_{sR}^q (dashed) and currents i_s^d and i_s^q (solid) for $L = 1.5L^{\text{nom}}$ (in [A]). (b) Current references i_{sR}^d and i_{sR}^q (dashed) and currents i_s^d and i_s^q (solid) for $L = 0.75L^{\text{nom}}$ (in [A]).

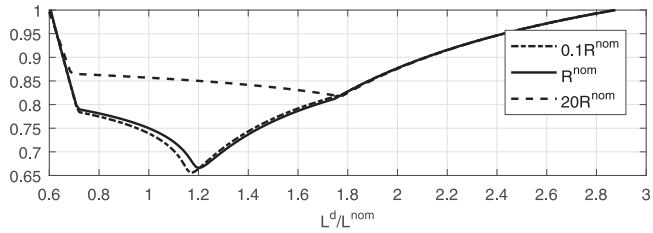

Fig. 8. Plot of (30) for $0.6L^{\text{nom}} < L^d < 3L^{\text{nom}}$ and three values of R^d.

were computed [22]. Defining signals $\vec{d}$ and $\vec{n}$ in Fig. 6(a), it results $S = \vec{i}_s^{d,q}/\vec{d}$ and $T = -\vec{i}_s^{d,q}/\vec{n}$. Fig. 6(a) is the same as Fig. 2(a), but considering $\vec{i}_{sR}^{d,q} = 0$. Signal $\vec{d}$ represents a perturbation current in system (4)–(5) produced by $\vec{v}_p^{\alpha,\beta}$ [defined in (3)]. Signal $\vec{d}$ has its main spectral components at specific harmonics of the fundamental grid frequency: $\pm 6h$ and $\pm 6h - 2$ with $h \in \mathbb{N}$, $h \geq 0$. Sensitivity function $S = \vec{i}_s^{d,q}/\vec{d}$ quantifies the controller's steady-state rejection capability to perturbation $\vec{d}$. For a given frequency, the smaller $|S|$, the greater the steady-state rejection. Fig. 6(b) shows $|S|$, for three different values of a_1. Note in Fig. 6(b) that reducing the value of a_1 improves the steady-state rejection for harmonic orders below 23, which is the range where most of the grid harmonic contamination is usually located. However, also notice that for smaller values of a_1, the rejection of harmonic orders above 23 is worse.

Signal $\vec{n}$ in Fig. 6(a) represents the measurement noise (a high-frequency signal). The complementary sensitivity function $T = -\vec{i}_s^{d,q}/\vec{n}$ quantifies the controller's rejection capability to measurement noise. For a given frequency, the smaller $|T|$, the greater the rejection. Fig. 6(c) shows $|T|$ for three different values of a_1. Notice that for smaller values of a_1, the rejection of high-frequency measurement noise is worse. In a practical application, low rejection of measurement noise results in control action saturation.

As stated previously, from (22), it is clear that for smaller values of a_1, the closed-loop response of the system to a variation in perturbation $\vec{v}_p^{\alpha,\beta}$ is faster. From the present analysis, it is also clear that reducing the value of a_1 improves the perturbation rejection for harmonic orders below 23. However, for smaller values of a_1, the rejection of higher frequency harmonics and measurement noise is worse. Therefore, when choosing the value of a_1, a compromise must be made between these facts.

B. Mismatch of Parameters

In what follows, we will initially evaluate by simulation the effect of a mismatch in the value of L on the temporary response of the closed-loop system. To evaluate this effect, controller gains $k_1 - k_4$ are designed using (18)–(21) considering that $L = L^{\text{nom}} = 4.5$ mH. Then, *Simulation 1* is repeated for two cases in which the value of L of the plant does not match with L^{nom}. Fig. 7(a) shows a detail of current references i_{sR}^d and i_{sR}^q (dashed line), along with currents i_s^d and i_s^q (solid lines) for the case where $L = 1.5L^{\text{nom}}$. Fig. 7(b) shows the same variables for the case where $L = 0.75L^{\text{nom}}$. In both figures, it is observed that the currents exhibit a settling time of approximately 18 samples, and that there is a slight coupling between the axes d and q. As expected, a mismatch in the value of L degrades the temporary response. However, the system remains stable in both cases.

In what follows, the limits of variation of L within which the system remains stable will be found, considering also variations in resistance R. To do so, controller gains $k_1 - k_4$ are designed using (18)–(21) considering that $L = L^{\text{nom}} = 4.5$ mH and $R = R^{\text{nom}} = 676.66$ mΩ. In the event that the value of L and R of the plant do not match L^{nom} and R^{nom}, but have value $L = L^d$ and $R = R^d$, it is easy to show, after some algebraic manipulation,

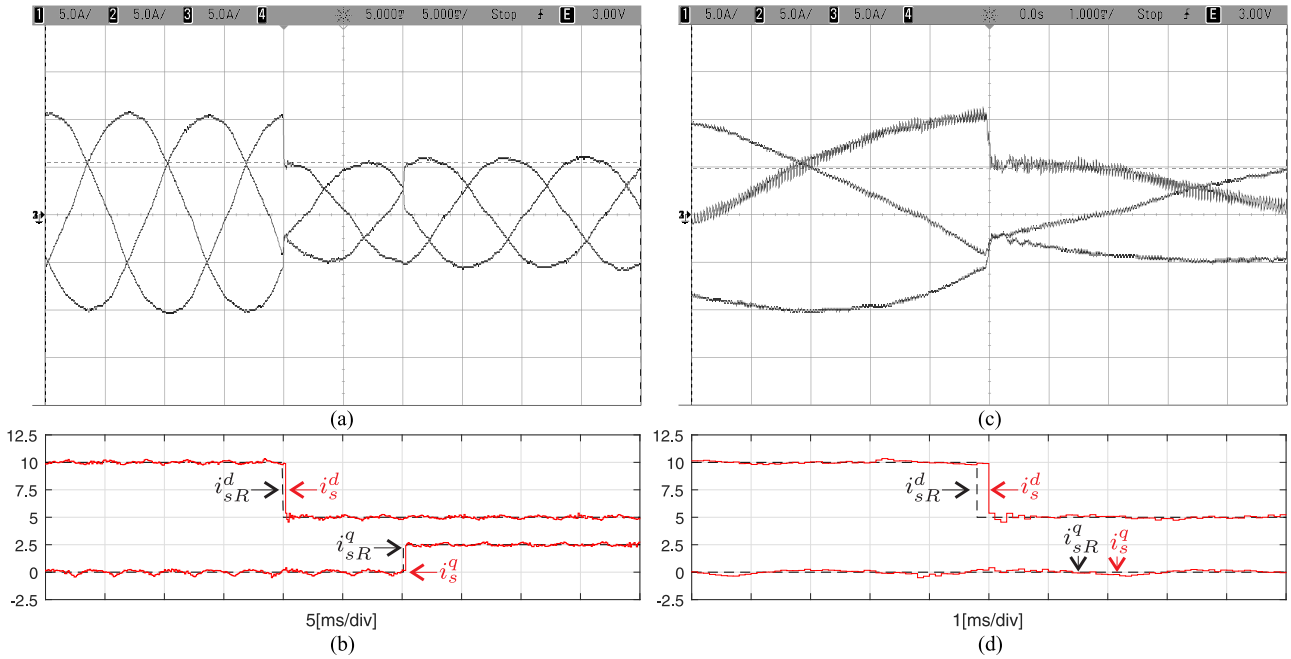

Fig. 9. Experimental results for the proposed controller to reference changes (timescale 5 ms/div). (a) Phase currents (scale 5 A/div). (b) Current references i^d_{sR} and i^q_{sR} (dashed) and currents i^d_s and i^q_s (solid) (in [A]). (c) and (d) zooms of (a) and (b).

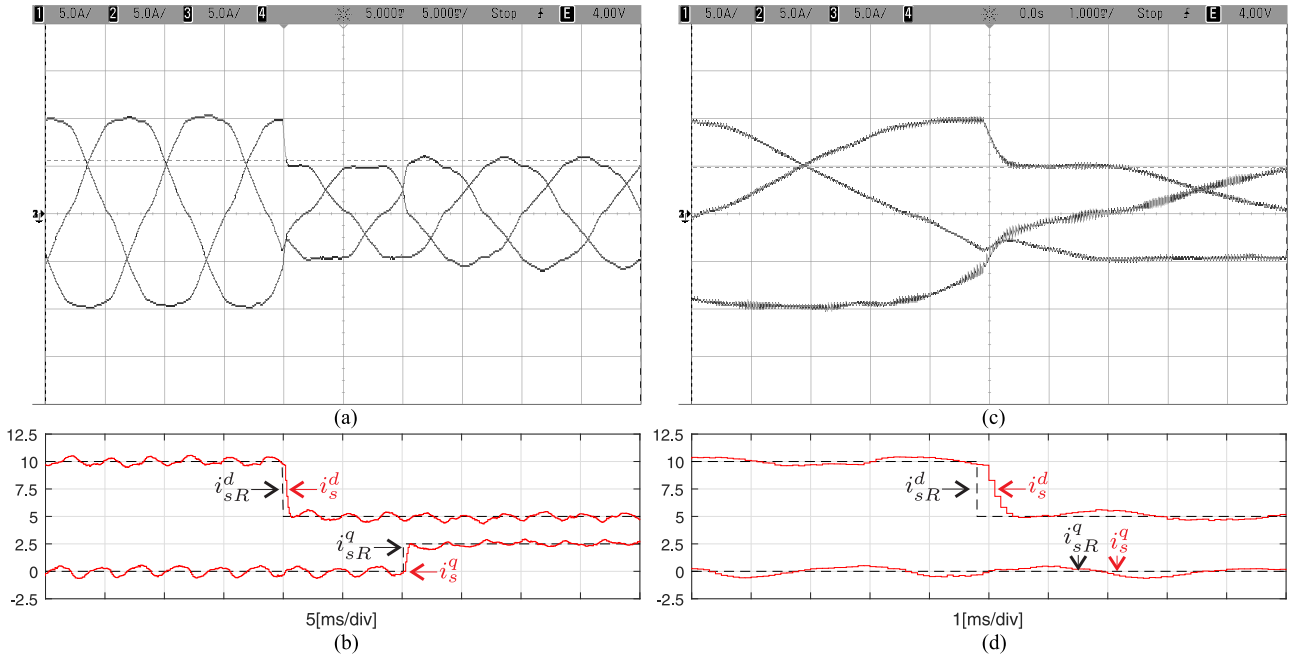

Fig. 10. Experimental results for controller (10) to reference changes (timescale 5 ms/div). (a) Phase currents (scale 5 A/div). (b) Current references i^d_{sR} and i^q_{sR} (dashed) and currents i^d_s and i^q_s (solid) (in [A]). (c) and (d) zooms of (a) and (b).

that the closed-loop transfer function of the system of Fig. 2(a) results

$$\frac{\vec{i}^{\,d,q}_s(z)}{\vec{i}^{\,d,q}_{sR}(z)} = \frac{k_4 k_3 b^d_{g1} b^d_{g2}(z-a_1)}{z^3 - c_1 z^2 + c_2 z - c_3} \tag{25}$$

where

$$c_1 = k_1 + a^d_g + 1 \tag{26}$$

$$c_2 = k_1 a^d_g + k_3 k_2 b^d_{g1} b^d_{g2} + k_1 + a^d_g + k_4 k_3 b^d_{g1} b^d_{g2} \tag{27}$$

$$c_3 = k_1 a^d_g + k_3 k_2 b^d_{g1} b^d_{g2} + a_1 k_4 k_3 b^d_{g1} b^d_{g2} \tag{28}$$

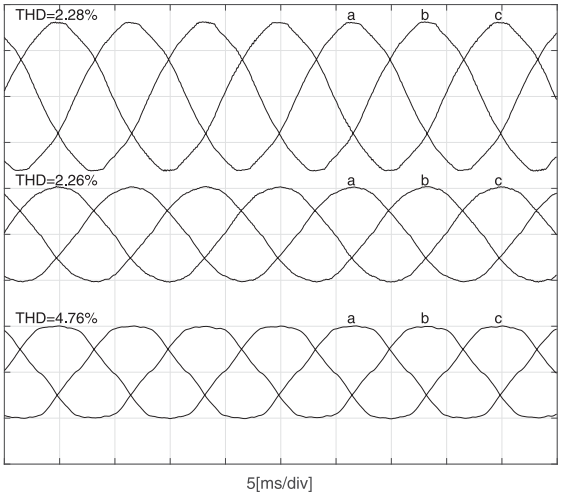

Fig. 11. Experimental results (timescale 5 ms/div). Phase voltages (top, scale 100 V/div), current injected by the proposed controller (middle, scale 10 A/div), and current injected by controller (10) (bottom, scale 10 A/div).

with a_g^d, b_{g1}^d, and b_{g2}^d computed through the right-hand side of (6)–(8), respectively, using $a = e^{-R^d T_s/L^d}$, $b = (1 - e^{-R^d T_s/L^d})/R^d$. For each value of L^d and R^d, the system will be stable as long as the roots p_1–p_3 of the denominator polynomial of (25)

$$\{p_1,\ p_2,\ p_3\} = \text{roots}(z^3 - c_1 z^2 + c_2 z - c_3) \tag{29}$$

are inside the unit circle. Defining

$$r = \max(|p_1|,\ |p_2|, |p_3|) \tag{30}$$

then, the system will be stable as long as $r < 1$.

Fig. 8 shows r as a function of L^d/L^{nom}, for $0.6L^{\text{nom}} < L^d < 3L^{\text{nom}}$, and three values of R^d ($0.1R^{\text{nom}}$, R^{nom}, and $20R^{\text{nom}}$). This figure shows that the closed-loop system remains stable for $0.61L^{\text{nom}} < L^d < 2.87L^{\text{nom}}$, independently of the value of R^d.

VI. Experimental Results

For the experimental results, the dc bus was supplied through a SORENSEN SGI 600/25 dc voltage source set to 400 V. The parameters of the output filter were the same as in the simulations: $L = 4.5$ mH and $R = 676.66$ mΩ. The grid voltage was 110 Vrms (obtained from the public grid through an isolation transformer) with fundamental angular frequency $\omega_g = 2\pi 50$ rad/s. The inverter was implemented using IRG4PH50UD IGBTs, with a turn ON dead time of 1 μs. The controller was implemented in a floating point DSP (TMS320F28335), using a sampling period $T_s = 100\,\mu$s. All the phase currents were captured using the oscilloscope in high-resolution mode (switching ripple filtered depending on the timescale), and all d, q currents were captured from the internal registers of the DSP (sampled once every 100 μs). For the proposed controller, the gains were computed through (18)–(21), using $a_1 = 0.75$. Controller (10) was implemented with $\gamma = 0.3$. As in the simulations, the feedforward voltage was proportional to the fundamental component of the grid voltage, provided by the SRF-PLL, $v_{ff}^{\alpha,\beta} = K\vec{v}_{s0}^{\alpha,\beta}$, where $K = 1$ unless otherwise stated.

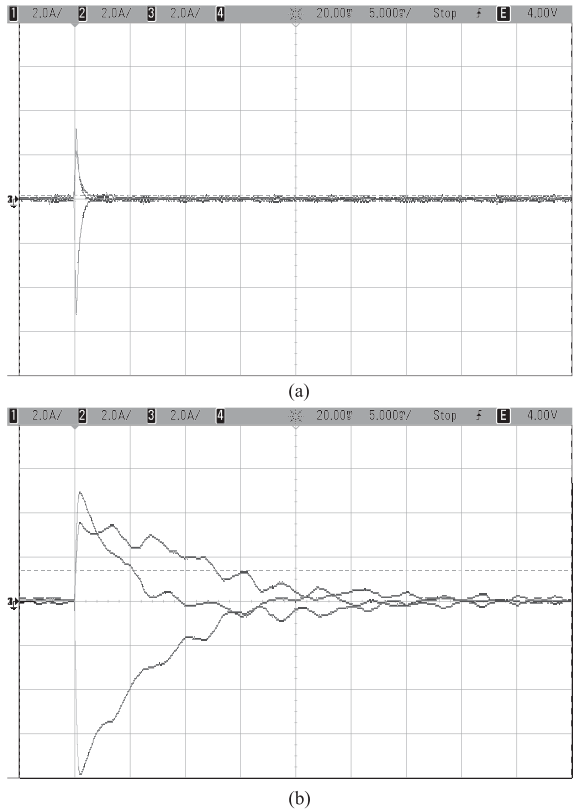

Fig. 12. Experimental results to a step change in K (timescale 5 ms/div). (a) Phase currents for the proposed controller (scale 2 A/div). (b) Phase currents for controller (10) (scale 2 A/div).

Fig. 9 experimentally verifies the simulation results shown in Fig. 3(a) and (b) (proposed controller). Fig. 9(a) shows the phase currents, and Fig. 9(c) shows a detail of these currents. Fig. 9(b) shows current references i_{sR}^d and i_{sR}^q (dashed line), along with currents i_s^d and i_s^q (solid line), and Fig. 9(d) shows a detail of these currents. At the beginning of the experiment, the inverter is injecting a peak current of 10 A per phase. As in the simulation results shown in Fig. 3(a) and (b), first current reference i_{sR}^d is reduced from 10 to 5 A, and 10 ms later, current reference i_{sR}^q is increased from 0 to 2.5 A. Fig. 9(b) and (d) verifies that currents i_s^d and i_s^q copy their references in two samples (200 μ s), and that the change in each variable is decoupled from the other.

Fig. 10 shows the same variables as shown in Fig. 9, but for controller (10). Varying the current references as in the previous experiment, Fig. 10(b) and (d) verifies that currents i_s^d and i_s^q copy their references within six samples, practically without overshoot, and in a perfectly decoupled way.

For the results shown in Fig. 11, both controllers were set to inject an active current of 10 A peak, and their steady-state harmonic contamination was measured. Fig. 11(top) shows the captured phase voltages. This grid's main harmonics were the 5th, 7th, 11th, and the 13th in the following percentages, respectively: 2.4%, 0.6%, 0.3%, and 0.3%. Fig. 11(middle) shows the phase currents injected by the proposed controller, which had an average THD = 2.26%. Fig. 11(bottom) shows the phase currents injected by controller (10), which has an average THD = 4.76%. It is verified that the proposed controller has better steady-state disturbance rejection capabilities than controller (10).

Fig. 12 shows the behavior of both controllers to a perturbation variation $\vec{v}_p^{\alpha,\beta}$. Here, current references i_{sR}^d and i_{sR}^q are both set to zero, and a step change in K of (24) is performed, jumping from $K = 1$ to $K = 0$. Fig. 12(a) shows the phase currents for the proposed controller, and Fig. 12(b) shows the phase currents for controller (10). It is, therefore, experimentally verified that the proposed controller is able to cancel the transient due to perturbation $\vec{v}_p^{\alpha,\beta}$ noticeably faster.

VII. Conclusion

This paper presents a new PI current controller structure implemented in a synchronous d, q reference frame for a grid-tied VSI. The proposed controller is formulated in discrete time, has dead beat response to reference changes, and offers full decoupling between axes d and q. The proposed controller is compared with the one SRF-PI recently presented in the literature. It is verified that beside having a dead beat response, the proposed controller introduces a noticeable improvement in the transient and steady-state responses to disturbances in the control loop.

References

[1] M. Ashabani and Y. A. R. I. Mohamed, "Integrating VSCS to weak grids by nonlinear power damping controller with self-synchronization capability," *IEEE Trans. Power Syst.*, vol. 29, no. 2, pp. 805–814, Mar. 2014.

[2] *IEEE Standard for Interconnecting Distributed Resources With Electric Power Systems*, IEEE Std 1547-2003, 2003.

[3] "Transmission code 2007. Networks and system rules of the German transmission system operators," VDN-e.v. beim VDEW, Berlin, Germany, Aug. 2007.

[4] "ENTSO-E network code for requirements for grid connection applicable to all generators," Eur. Netw. Transmiss. Syst. Operators Elect. Doc., Brussels, Belgium, Jun. 2012.

[5] S. Buso, T. Caldognetto, and D. I. Brandao, "Dead-beat current controller for voltage-source converters with improved large-signal response," *IEEE Trans. Ind. Appl.*, vol. 52, no. 2, pp. 1588–1596, Mar. 2016.

[6] L. Malesani, P. Mattavelli, and S. Buso, "Robust dead-beat current control for PWM rectifiers and active filters," *IEEE Trans. Ind. Appl.*, vol. 35, no. 3, pp. 613–620, May 1999.

[7] J. C. Moreno, J. M. E. Huerta, R. G. Gil, and S. A. Gonzalez, "A robust predictive current control for three-phase grid-connected inverters," *IEEE Trans. Ind. Electron.*, vol. 56, no. 6, pp. 1993–2004, Jun. 2009.

[8] J. M. Espi, J. Castello, R. García-Gil, G. Garcera, and E. Figueres, "An adaptive robust predictive current control for three-phase grid-connected inverters," *IEEE Trans. Ind. Electron.*, vol. 58, no. 8, pp. 3537–3546, Aug. 2011.

[9] A. Kuperman, "Proportional-resonant current controllers design based on desired transient performance," *IEEE Trans. Power Electron.*, vol. 30, no. 10, pp. 5341–5345, Oct. 2015.

[10] A. Vidal *et al.*, "Assessment and optimization of the transient response of proportional-resonant current controllers for distributed power generation systems," *IEEE Trans. Ind. Electron.*, vol. 60, no. 4, pp. 1367–1383, Apr. 2013.

[11] A. Vidal, F. Freijedo, A. Yepes, J. Malvar, O. Lopez, and J. Doval-Gandoy, "Transient response evaluation of stationary-frame resonant current controllers for grid-connected applications," *IET Power Electron.*, vol. 7, no. 7, pp. 1714–1724, Jul. 2014.

[12] C. A. Busada, S. G. Jorge, and J. A. Solsona, "Resonant current controller with enhanced transient response for grid-tied inverters," *IEEE Trans. Ind. Electron.*, vol. 65, no. 4, pp. 2935–2944, Apr. 2018.

[13] Q. N. Trinh, F. H. Choo, and P. Wang, "Control strategy to eliminate impact of voltage measurement errors on grid current performance of three-phase grid-connected inverters," *IEEE Trans. Ind. Electron.*, vol. 64, no. 9, pp. 7508–7519, Sep. 2017.

[14] J. Holtz, J. Quan, J. Pontt, J. Rodriguez, P. Newman, and H. Miranda, "Design of fast and robust current regulators for high-power drives based on complex state variables," *IEEE Trans. Ind. Appl.*, vol. 40, no. 5, pp. 1388–1397, Sep. 2004.

[15] A. G. Yepes, A. Vidal, O. López, and J. Doval-Gandoy, "Evaluation of techniques for cross-coupling decoupling between orthogonal axes in double synchronous reference frame current control," *IEEE Trans. Ind. Electron.*, vol. 61, no. 7, pp. 3527–3531, Jul. 2014.

[16] A. G. Yepes, A. Vidal, J. Malvar, O. López, and J. Doval-Gandoy, "Tuning method aimed at optimized settling time and overshoot for synchronous proportional-integral current control in electric machines," *IEEE Trans. Power Electron.*, vol. 29, no. 6, pp. 3041–3054, Jun. 2014.

[17] H. Kim, M. W. Degner, J. M. Guerrero, F. Briz, and R. D. Lorenz, "Discrete-time current regulator design for ac machine drives," *IEEE Trans. Ind. Appl.*, vol. 46, no. 4, pp. 1425–1435, Jul. 2010.

[18] N. Hoffmann, F. W. Fuchs, M. P. Kazmierkowski, and D. Schröder, "Digital current control in a rotating reference frame - Part I: System modeling and the discrete time-domain current controller with improved decoupling capabilities," *IEEE Trans. Power Electron.*, vol. 31, no. 7, pp. 5290–5305, Jul. 2016.

[19] C. A. Busada, S. G. Jorge, and J. A. Solsona, "Comments on 'digital current control in a rotating reference frame - Part I: System modeling and the discrete time-domain current controller with improved decoupling capabilities'," *IEEE Trans. Power Electron.*, vol. 34, no. 3, pp. 2980–2984, Mar. 2019.

[20] R. J. Vaccaro, *Digital Control. A State-Space Approach*. New York, NY, USA: McGraw-Hill, 1995.

[21] J. Rocabert, A. Luna, F. Blaabjerg, and P. Rodríguez, "Control of power converters in ac microgrids," *IEEE Trans. Power Electron.*, vol. 7, no. 11, pp. 4734–4749, Nov. 2012.

[22] K. Åström and R. Murray, *Feedback Systems: An Introduction for Scientists and Engineers*. Princeton, NJ, USA: Princeton Univ. Press, 2008.

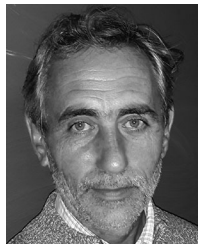

Claudio A. Busada was born on March 13, 1962, in Bahia Blanca, Argentina. He received the Electrical Engineer degree, in 1989 and the Ph.D. degree in control systems, in 2004, both from the Universidad Nacional del Sur, Bahía Blanca, Argentina.

From 1988 to 2004, he was with the Mechanic and Electrical Department, Bahia Blanca. Since 1989, he has been with the Departamento de Ingenieria Electrica y de Computadoras, Universidad Nacional del Sur, Bahía Blanca, Argentina, where he is a Professor. He is a Researcher with the Instituto de Investigaciones en Ingenieria Electrica "Alfredo C. Desages," Bahía Blanca, Argentina. His research interests include power electronics, rotating machinery, active filters, automatic control, and integration of distributed energy systems.

Sebastian Gomez Jorge received the Electronics Engineer, M.S. degree in electrical engineering, and Ph.D. degree in engineering from the Universidad Nacional del Sur, Bahía Blanca, Argentina, in 2006, 2009, and 2011, respectively.

He is currently with CONICET, Instituto de Investigaciones en Ingenieria Electrica "Alfredo C. Desages," and with the Departamento de Ingenieria Electrica y de Computadoras of Universidad Nacional del Sur, Bahia Blanca, Argentina, where he is a Graduate Teaching Assistant.

Jorge A. Solsona (SM'04) received the Electronics Engineer degree and the Ph.D. degree in engineering from the Universidad de La Plata, La Plata, Argentina, in 1986 and 1995, respectively.

He is currently with the Departamento de Ingenieria Electrica y de Computadoras, Instituto de Investigaciones en Ingenieria Electrica "Alfredo C. Desages" (IIIE), Universidad Nacional del Sur, Bahia Blanca, Argentina, where he is a Professor, and also with CONICET, Argentina. He is involved in teaching and research on control theory and its applications to electromechanical systems.